Localization of Passive 3-D Coils as an Inverse Problem: Theoretical Analysis and a Numerical Method

Martin Doß[1], Leon Bungert[2], Daniel Cichon[3], Hartmut Brauer[4], and Rafael Psiuk[1]

[1]Department of Self-Powered Radio Systems, Fraunhofer Institute for Integrated Circuits, 90411 Nürnberg, Germany
[2]Department of Mathematics, Friedrich–Alexander Universität Erlangen-Nürnberg, 91058 Erlangen, Germany
[3]Department of Integrated Sensor Systems, Fraunhofer Institute for Integrated Circuits, 91058 Erlangen, Germany
[4]Advanced Electromagnetics Group, Technische Universität Ilmenau, 98693 Ilmenau, Germany

This article provides both a theoretical analysis and a numerical method for the inverse source problem of locating multiple passive 3-D coils based on measurements of their superposed magnetic fields. In our context, a 3-D coil consists of three concentric circular coils being mutually perpendicular, and the term "passive" means that these coils are not connected to an active power source. Instead, their current is induced externally by a low-frequency alternating magnetic field which is generated by a closed exciter wire. The underlying inductively coupled system is modeled with regard to the 3-D coils as magnetic dipoles and their localization is formulated as an inverse problem. Since its ill posedness mainly arises from strong sensitivity to observational noise, an approximate upper bound for the localization error is derived mathematically by linearization. The Levenberg–Marquardt algorithm is applied as a method for localization and modified for better performance as well as the ability to estimate the number of 3-D coils in the localization area. Our method is tested with simulated and real data in order to confirm its capability of locating up to three passive 3-D coils within the front of a wooden shelf surrounded by the exciter wire and eight rectangular loop antennas.

Index Terms— **3-D coil, inverse problem, Levenberg–Marquardt algorithm, magnetic dipole, magnetic source localization.**

I. Introduction

DISTRIBUTION centers are required to operate as reliable and error free as possible in order to guarantee a resilient flow of goods. Fully automated warehouses are, however, very cost intensive and also inflexible to changes in the distribution process. Therefore, the human worker remains an integral part of every supply network. Of course, mistakes can be made when picking goods from the shelves according to the customers' order by hand. In Industry 4.0, this problem is addressed by supporting the worker with audiovisual technologies like headsets [1] or Augmented Reality [2].

In this article, we provide the technical foundation for a smart shelf giving positive or negative feedback whether some item is picked from the right compartment or not. The technology is based on the localization of the worker's hands within the front plane of the shelf. For this purpose, each of his wrists is equipped with a so-called 3-D coil consisting of three small circular coils which are aligned perpendicular to each other. If supplied with electric current, the 3-D coils generate a magnetic field that can be measured in order to determine their positions. The originality of our approach arises from the fact that the 3-D coils are not connected to an active power source but inductively supplied with current. For this purpose, a closed wire is placed around the front of the shelf and connected to a source of alternating current at low frequency in order to generate an oscillating magnetic field. To linguistically distinguish this field from the one generated by the 3-D coils, we, respectively, name them primary and secondary magnetic fields. All 3-D coils are tuned to be in resonance with the primary field's frequency by capacitors. Several rectangular loop antennas are placed around the front of the shelf measuring the secondary field's magnetic flux through their surfaces by induction. In the following, we refer to these antennas as pickup coils [3] and to the closed wire generating the primary field as the exciter wire. Since the picking process usually requires both hands, our method has to be capable of locating at least two 3-D coils at the same time. However, there is no need to distinguish the right from the left hand.

The localization of passive 3-D coils was proposed by the Fraunhofer Institute for Integrated Circuits (IIS) as part of the goal-line technology GoalRef [4], [5] certified by the Fédération Internationale de Football Association (FIFA). For the detection of goal events, a 3-D coil is integrated into the soccer ball. In [6], a modified version of GoalRef known as the IndLoc positioning system is used to perform full 2-D localization of multiple 3-D coils within a wooden shelf. The IndLoc localization algorithm is based on simple fingerprinting and orthogonal codes are used to separate the magnetic fields generated by the different 3-D coils. In [7], it is analyzed how the localization accuracy is affected by the arbitrary orientation of the passive 3-D coil.

In this article, we present an alternative localization algorithm based on methods from nonlinear optimization instead of fingerprinting. Our method is also capable of locating multiple 3-D coils without separating their signals. By that, the manufacturing costs for the 3-D coils are reduced since the use of additional signal processing devices as given in [6] is no longer required.

Manuscript received August 10, 2019; revised October 25, 2019; accepted January 17, 2020. Date of publication January 23, 2020; date of current version March 18, 2020. Corresponding author: M. Doß (e-mail: dossmn@iis.fraunhofer.de).

Color versions of one or more of the figures in this article are available online at http://ieeexplore.ieee.org.

Digital Object Identifier 10.1109/TMAG.2020.2968858

Apart from the previous works by Fraunhofer, magnetic source localization plays an important role in many current research areas. Whenever some object generates a magnetic field, the latter can be measured in order to determine the object's position. Although this basic concept is always the same, there is a broad spectrum of possible scenarios, and the differences in the technical details can be very subtle. First, the magnetic sources vary from permanent magnets [8] over electrical activities in the human brain [9] to current-carrying coils [10]. In the last case—which is of special interest to us—the coils are usually attached to the objects to be localized. In some applications, these coils are flat [11] whereas in others multiple coils are combined to a three-dimensional array [12], [13]. Regardless of their shape, the electric current is always required to generate a magnetic field. In [14], this is realized by connecting them to an active power source. The localization of a resonant magnetic marker is described in [15]. Every localization algorithm is based on a physical model describing the relation between the magnetic source and its field measurements. Coils are usually treated as magnetic dipoles. From a mathematical point of view, the actual localization is then performed by solving an inverse problem which is achieved by optimization algorithms like Levenberg–Marquardt [16] or unscented Kalman filter [17]. If multiple coils are supposed to be positioned at the same time, they can be tuned to different frequencies in order to separate their signals as shown in [18]. By that, the same localization algorithms as in the case of a single coil apply.

In our case, all 3-D coils are tuned to the same resonance frequency and only their cumulative field is measured. Hence, our localization algorithm has to be capable of fitting multiple dipoles simultaneously to the measured data. Similar algorithms are used in magnetoencephalography (MEG) to map human brain activity [19]. Also, in [20]–[23] the electromagnetic radiation of an electronic device is determined by fitting a set of electric and magnetic dipoles to measurements of its near field.

This article is structured as follows: first, a model is derived in Section II describing the inductive coupling between all components of the system. In Section III, the localization of multiple passive 3-D coils is embedded into the mathematical theory of inverse problems which also includes the discussion of the term "ill posedness" in our context. After these theoretical considerations, the Levenberg–Marquardt algorithm is introduced as a method for localization in Section IV. The algorithm's performance and its sensitivity to observational Gaussian noise are both tested with simulated data in Section V. The smart shelf from [6] is then used to verify the functionality of our localization method with real data in Section VI. Finally, Section VII concludes this article.

II. Forward Model

Understanding the passive 3-D coils' inductive coupling with the primary magnetic field and the pickup coils is fundamental for their localization. Our aim is to predict the induced voltages at the pickup coils as functions of the 3-D coil positions. In order to do so, the model in [5] is simplified by treating the 3-D coils as magnetic dipoles. Since we are only interested in peak values of voltages and currents in our calculations, it is sufficient to treat them as real numbers. Furthermore, vectors are printed bold for better readability.

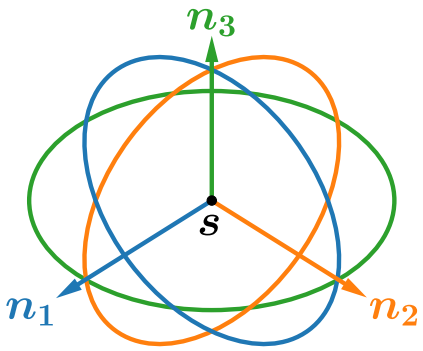

Fig. 1. Three orthogonal circular coils forming a 3-D coil with their respective unit normal vectors $\boldsymbol{n_1}, \boldsymbol{n_2}, \boldsymbol{n_3}$ (in the same color) and common center $\boldsymbol{s}$.

Let $P \subset \mathbb{R}^3$ be the set of admissible 3-D coil positions. A closed exciter wire E is placed outside P and connected to a current source with amplitude I_{ex} and low frequency f in order to generate an oscillating primary magnetic field inductively supplying the 3-D coils with current. The vector-valued amplitude of its flux density $\boldsymbol{B^1}$ at position $\boldsymbol{p} \in \mathbb{R}^3$ is described by the Biot–Savart law [24]

$$\boldsymbol{B^1}(\boldsymbol{p}) = -\frac{\mu_0 I_{\text{ex}}}{4\pi} \oint_E \frac{(\boldsymbol{p}-\boldsymbol{p'}) \times d\boldsymbol{p'}}{\|\boldsymbol{p}-\boldsymbol{p'}\|^3} \tag{1}$$

where μ_0 denotes the vacuum permeability and $d\boldsymbol{p'}$ an infinitesimal wire element tangential to E at position $\boldsymbol{p'}$. Note that this formula only applies to direct current as well as alternating current of low frequency for which a quasistatic approximation is possible. A 3-D coil consists of three mutually perpendicular concentric circular coils which are assumed to be identical in their area S and their number of windings N. Each circular coil is tuned to be in resonance with the exciter frequency f by means of capacitors being soldered in series to the coil according to Thomson's formula [25, Ch. 14.5]

$$f = \frac{1}{2\pi\sqrt{LC}} \tag{2}$$

where L and C denote inductance and capacitance, respectively, of each circular coil. The geometry of a 3-D coil is uniquely determined by a common center $\boldsymbol{s} \in P$ of its circular coils as well as their unit normal vectors $\boldsymbol{n_1}, \boldsymbol{n_2}, \boldsymbol{n_3}$ being perpendicular to the corresponding surfaces S_1, S_2, S_3 as shown in Fig. 1. The flux density of the primary magnetic field passing through a 3-D coil is approximated by its linearization in the center $\boldsymbol{s}$

$$\boldsymbol{B^1}(\boldsymbol{p}) \approx \boldsymbol{B^1}(\boldsymbol{s}) + D\boldsymbol{B^1}(\boldsymbol{s})(\boldsymbol{p}-\boldsymbol{s}) \tag{3}$$

where $D\boldsymbol{B^1}(\boldsymbol{s})$ denotes the Jacobian matrix of $\boldsymbol{B^1}$ evaluated at $\boldsymbol{s}$. Hence, if S is sufficiently small, we can approximate the primary field's magnetic flux Φ_α through the αth circular coil belonging to a 3D-coil with center $\boldsymbol{s}$ as

$$\begin{aligned}\Phi_\alpha &= \iint_{S_\alpha} \boldsymbol{B^1}(\boldsymbol{p}) \cdot \boldsymbol{n_\alpha}\, dA(\boldsymbol{p}) \\ &\overset{(3)}{\approx} S\,\boldsymbol{B^1}(\boldsymbol{s}) \cdot \boldsymbol{n_\alpha} + \boldsymbol{n_\alpha}^T D\boldsymbol{B^1}(\boldsymbol{s}) \iint_{S_\alpha} \boldsymbol{p}-\boldsymbol{s}\, dA(\boldsymbol{p}) \\ &= S\,\boldsymbol{B^1}(\boldsymbol{s}) \cdot \boldsymbol{n_\alpha}\end{aligned} \tag{4}$$

taking into account that the surface integral of $\boldsymbol{p}-\boldsymbol{s}$ over the disk S_α vanishes due to its central symmetry with respect to $\boldsymbol{s}$. Due to Faraday's law of induction the induced peak voltage at the same circular coil is then obtained as

$$U_\alpha \approx -2\pi f N S\, \boldsymbol{B^1}(\boldsymbol{s}) \cdot \boldsymbol{n_\alpha}. \tag{5}$$

From (2), it follows that the impedance Z of each circular coil is purely resistive:

$$Z = R + j\left(2\pi f L - \frac{1}{2\pi f C}\right) = R \tag{6}$$

where R denotes the ohmic resistance which is assumed to be the same for all circular coils. Hence, the corresponding current at resonance can be calculated as

$$I_\alpha = \frac{U_\alpha}{R}. \tag{7}$$

According to [26, Ch. 29.5], we treat each circular coil as a magnetic dipole with the following dipole moment:

$$\boldsymbol{m_\alpha} = N I_\alpha S\, \boldsymbol{n_\alpha}. \tag{8}$$

The total dipole moment $\boldsymbol{m}(\boldsymbol{s})$ of a 3-D coil at position $\boldsymbol{s}$ is then obtained as the sum of these single dipole moments. Taking into account that $(\boldsymbol{n_1}, \boldsymbol{n_2}, \boldsymbol{n_3})$ is an orthonormal basis for $\mathbb{R}^3$ [27, Ch. 4.4], we obtain the following simple formula:

$$\begin{aligned}
\boldsymbol{m}(\boldsymbol{s}) &= \sum_{\alpha=1}^{3} \boldsymbol{m_\alpha} \\
&= NS \sum_{\alpha=1}^{3} I_\alpha \boldsymbol{n_\alpha} \\
&= \frac{NS}{R} \sum_{\alpha=1}^{3} U_\alpha \boldsymbol{n_\alpha} \\
&\approx -\frac{2\pi f N^2 S^2}{R} \sum_{i=1}^{3} (\boldsymbol{B^1}(\boldsymbol{s}) \cdot \boldsymbol{n_\alpha})\, \boldsymbol{n_\alpha} \\
&= -\frac{2\pi f N^2 S^2}{R} \boldsymbol{B^1}(\boldsymbol{s}).
\end{aligned} \tag{9}$$

So, in our model the total dipole moment does not depend on the 3-D coil's orientation and is already uniquely determined by its position. Of course, we could also use Taylor polynomials of higher order in the approximation of the primary field's flux density (3) or do not approximate it at all in order to increase the accuracy of our model. However, in this case the total dipole moment of a 3-D coil would also depend on its orientation and localization would not be possible without estimating the orientations of the 3-D coils which is not the purpose of our method.

The flux density of the secondary magnetic field generated by a passive 3-D coil with center $\boldsymbol{s}$ is denoted by $\boldsymbol{B_s^2}$ and its vector-valued amplitude at position $\boldsymbol{p} \in \mathbb{R}^3$ is described by [10]

$$\boldsymbol{B_s^2}(\boldsymbol{p}) = \frac{\mu_0}{4\pi}\left[\frac{3(\boldsymbol{p}-\boldsymbol{s})(\boldsymbol{m}(\boldsymbol{s}) \cdot (\boldsymbol{p}-\boldsymbol{s}))}{\|\boldsymbol{p}-\boldsymbol{s}\|^5} - \frac{\boldsymbol{m}(\boldsymbol{s})}{\|\boldsymbol{p}-\boldsymbol{s}\|^3}\right]. \tag{10}$$

Note that this formula is linear in $\boldsymbol{m}(\boldsymbol{s})$ which corresponds to the superposition principle for magnetic fields. The latter also states that the secondary fields of multiple 3-D coils overlap additively.

Now, let k be the number of pickup coils by which the total secondary field is measured. Surface and unit normal vector of the jth pickup coil are denoted by A_j and $\boldsymbol{a_j}$, respectively. The number of windings M is assumed to be the same for all pickup coils. If a 3-D coil is located at position $\boldsymbol{s}$, its secondary magnetic field induces the following voltage at the jth pickup coil:

$$U_j(\boldsymbol{s}) = -2\pi f M \iint_{A_j} \boldsymbol{B_s^2}(\boldsymbol{p}) \cdot \boldsymbol{a_j}\, dA(\boldsymbol{p}) \tag{11}$$

taking into account Faraday's law of induction. To ensure that the integral on the right-hand side of (11) is finite, we demand that the closures of all sets A_j do not intersect with the closure of P.

So far, only one 3-D coil was considered to be in the localization area at a time. The general case with multiple 3-D coils of identical design is derived easily: if l 3-D coils are located at the positions $\boldsymbol{s_1}, \ldots, \boldsymbol{s_l} \in P$, their total secondary magnetic field induces the following voltage at the jth pickup coil:

$$\sum_{i=1}^{l} U_j(\boldsymbol{s_i}). \tag{12}$$

In these calculations, the mutual inductance of the 3-D coils is neglected, i.e., we assume that the secondary field of one 3-D coil does not induce a current in another. Apart from the secondary magnetic field, the primary field also induces a voltage in the pickup coils. However, for a fixed geometrical setup this can be seen as a constant offset and by subtracting it from the total voltage we make sure that only the secondary field is measured. Note that the pickup coils also generate magnetic fields which are not respected by our model due to their negligibly small order of magnitude compared to the primary magnetic field. Both effects are minimized at our setup by placing the exciter wire along the symmetry axes of the pickup coils.

The voltages at the pickup coils are treated as components of a vector-valued function $\boldsymbol{F_l} : P^l \to \mathbb{R}^k$ defined by

$$\boldsymbol{F_l}(\boldsymbol{s_1}, \ldots, \boldsymbol{s_l}) := \sum_{i=1}^{l} \begin{pmatrix} U_1(\boldsymbol{s_i}) \\ \vdots \\ U_k(\boldsymbol{s_i}) \end{pmatrix} \tag{13}$$

where P^l denotes the l-fold Cartesian product $P \times \cdots \times P$. We refer to (13) as our forward model (for l 3-D coils). Due to its additivity

$$\boldsymbol{F_l}(\boldsymbol{s_1}, \ldots, \boldsymbol{s_l}) = \sum_{i=1}^{l} \boldsymbol{F_1}(\boldsymbol{s_i}) \tag{14}$$

we have

$$\boldsymbol{F_l}(\boldsymbol{s_1}, \ldots, \boldsymbol{s_l}) = \boldsymbol{F_l}(\boldsymbol{s_{\sigma(1)}}, \ldots, \boldsymbol{s_{\sigma(l)}}) \tag{15}$$

for all permutations σ on the set of indices $\{1, \ldots, l\}$. This equation can be seen as the mathematical analog to the fact that all 3-D coils are identically designed and therefore cannot be distinguished by their secondary magnetic fields.

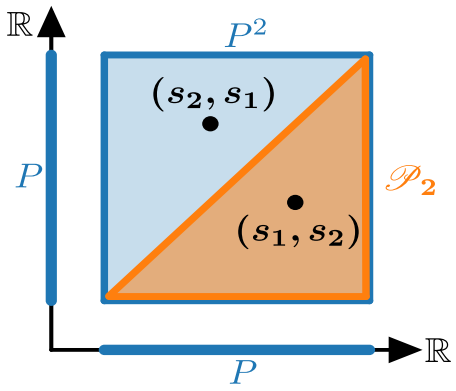

Fig. 2. Illustration of the set $\mathscr{P}_2$ for a 1-D position space P: in this case, the permutation of two 3-D coil positions $\boldsymbol{s_1}$ and $\boldsymbol{s_2}$ is equivalent to reflecting the respective tuple $(\boldsymbol{s_1}, \boldsymbol{s_2})$ across the diagonal of the product space P^2.

In order to eliminate these unintended ambiguities, we say that two l-tuples of positions $(\boldsymbol{s_1}, \ldots, \boldsymbol{s_l}), (\boldsymbol{s'_1}, \ldots, \boldsymbol{s'_l}) \in P^l$ are equivalent if and only if there is a permutation σ such that

$$(\boldsymbol{s_{\sigma(1)}}, \ldots, \boldsymbol{s_{\sigma(l)}}) = (\boldsymbol{s'_1}, \ldots, \boldsymbol{s'_l}). \tag{16}$$

The resulting equivalence relation $\sim$ is used to factorize the domain of $\boldsymbol{F_l}$ as

$$\mathscr{P}_l := P^l / \sim \tag{17}$$

where $P^l / \sim$ denotes the quotient space [28, Ch. 9]. In other words, the set $\mathscr{P}_l$ contains all combinations of l 3-D coil positions without respecting their order. If P is 1-D, the factorization of P^l to $\mathscr{P}_l$ is equivalent to the postulation $\boldsymbol{s_1} \leq \cdots \leq \boldsymbol{s_l}$ for all tuples $(\boldsymbol{s_1}, \ldots, \boldsymbol{s_l}) \in P^l$ as illustrated in Fig. 2. The invariance under permutation (15) ensures the well-definedness of $\boldsymbol{F_l}$ as a function over $\mathscr{P}_l$ (see also the universal property of the quotient space [28, Ch. 9]). In the following, we sometimes write $\boldsymbol{x} \in \mathscr{P}_l$ instead of $(\boldsymbol{s_1}, \ldots, \boldsymbol{s_l}) \in \mathscr{P}_l$ to make the notation more compact.

III. Localization as an Ill Posed Inverse Problem

Whenever cause is determined by effect, one speaks of an inverse problem. In this context, the measured voltages at the pickup coils are regarded as entries of a vector $\boldsymbol{b} \in \mathbb{R}^k$ and referred to as real or observational data. On the other hand, model data is generated as $\boldsymbol{F_l}(\boldsymbol{x})$ by evaluation of the forward model. Localization is then achieved by minimizing the discrepancy between real and model data. If the number l of 3-D coils in the localization area is known *a priori*, the residual

$$\|\boldsymbol{F_l}(\boldsymbol{x}) - \boldsymbol{b}\|_2 \tag{18}$$

is minimized over $\boldsymbol{x} \in \mathscr{P}_l$. Otherwise, this is done for all $l \in \{0, \ldots, l_{\max}\}$, and the best minimum with the smallest residual (18) is selected.

With this mathematical formulation of our localization problem several questions arise in a natural way: Does a solution always exist and if yes, is it unique? How sensitive is the localization of observational errors? All this can be summarized by the term well posedness which goes back to Hadamard [29]. According to him, a problem is said to be well posed if it satisfies the following three properties.

1) *Existence:* There is always at least one solution.
2) *Uniqueness:* There is always at most one solution.
3) *Stability:* The solution depends continuously on the data.

If just one of these three conditions is not fulfilled, the problem is called ill posed. The well/ill posedness of magnetic field localization is discussed in the following.

A. Existence

To make sure that (18) always attains its minimum in $\mathscr{P}_l$, we have to assume that the localization area P is a compact subset of $\mathbb{R}^3$. This constraint is reasonable in our context since it only requires P to be bounded and closed. The first Hadamard condition then follows from the extreme value theorem [30, Th. 4.16].

Theorem 1: Let K be a compact space and $\varphi : K \to \mathbb{R}$ a continuous function. Then there exists $\boldsymbol{x} \in K$ such that $\varphi(\boldsymbol{x}) = \inf \varphi(K)$.

More precisely, we choose $\varphi(\boldsymbol{x}) = \|\boldsymbol{F_l}(\boldsymbol{x}) - \boldsymbol{b}\|_2$ and $K = \mathscr{P}_l$. The compactness of $\mathscr{P}_l$ follows from Tychonoff's theorem and the fact that the quotient space of a compact space is still compact [28, Ch. 17]. φ is continuous as a composition of continuous functions (for the continuity of $\boldsymbol{F_l}$ see also the universal property of the quotient space [28, Ch. 9]).

B. Uniqueness

Since our forward model is nonlinear and not surjective in general, minima of (18) are not always unique. This can be seen from the following simple example: consider the 1D-localization of a single passive 3-D coil along the x-axis by means of two identical circular pickup coils both lying in the xy-plane at the same distance from the x-axis. If the primary magnetic field is homogenous along the x-axis and pointing in the z-direction, the forward model (13) can be written as

$$\boldsymbol{F_1}(\boldsymbol{s}) = \begin{pmatrix} \int_{A_1} \frac{C}{\|\boldsymbol{p}-\boldsymbol{s}\|^3}\, dA(\boldsymbol{p}) \\ \int_{A_2} \frac{C}{\|\boldsymbol{p}-\boldsymbol{s}\|^3}\, dA(\boldsymbol{p}) \end{pmatrix} \tag{19}$$

with some constant $C > 0$. Plotting the image of $\boldsymbol{F_1}$ as a subset of $\mathbb{R}^2$ indicates the existence of a measurement $\boldsymbol{b} \in \mathbb{R}^2$ for which (18) attains its minimum at three different 3-D coil positions $\boldsymbol{s^*}$, $\boldsymbol{s^{**}}$, $\boldsymbol{s^{***}}$. Fig. 3 illustrates the example.

C. Stability

From a geometric point of view two operations are performed when minimizing the residual (18): first, the observational data $\boldsymbol{b} \in \mathbb{R}^k$ are projected onto the image of the forward model in the sense that the projection $\boldsymbol{b^*} \in \boldsymbol{F_l}(\mathscr{P}_l)$ has minimum Euclidean distance to $\boldsymbol{b}$. Then every $\boldsymbol{x^*} \in \mathscr{P}_l$ with the property $\boldsymbol{F_l}(\boldsymbol{x^*}) = \boldsymbol{b^*}$, i.e., every preimage of the projection, is a solution of the inverse problem. Thus, the solution only depends continuously on the data if both projection and mapping to the preimage are continuous. In the previous example, we have already seen that discontinuities in the projection are possible: near $\boldsymbol{b}$ the projection of the data onto $\boldsymbol{F_1}(P)$ jumps between $\boldsymbol{b^*}$, $\boldsymbol{b^{**}}$, and $\boldsymbol{b^{***}}$. However, it can be shown that preimages always depend continuously on their

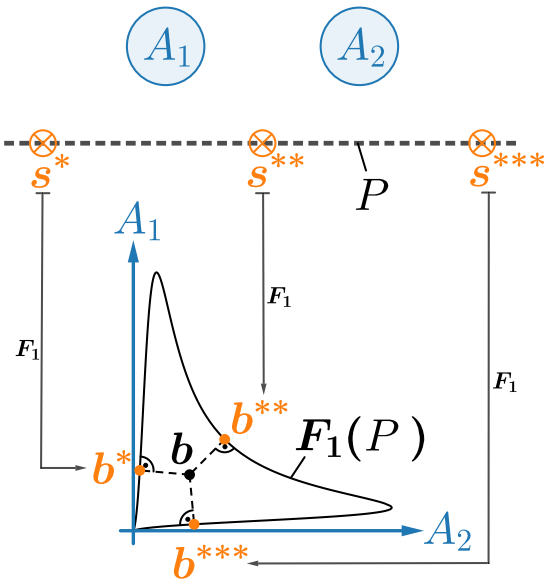

Fig. 3. Counterexample for the second Hadamard condition: consider the 1-D localization of a single passive 3-D coil along a straight line P with homogenous primary magnetic field by means of two circular pickup coils A_1 and A_2 as shown in the upper half of the figure. The model data for this setup is visualized by plotting the image of (19) as a subset of $\mathbb{R}^2$. Due to its geometry, there exists a measurement $\boldsymbol{b}$ having minimal Euclidean distance to $\boldsymbol{F_1}(P)$ at three different image points $\boldsymbol{b^*}$, $\boldsymbol{b^{**}}$, $\boldsymbol{b^{***}}$. The corresponding preimages $\boldsymbol{s^*}$, $\boldsymbol{s^{**}}$, $\boldsymbol{s^{***}}$ are the solutions of the inverse problem.

images if the forward model is continuous and injective. This statement is a basic theorem from topology [28, Ch. 17].

Theorem 2: Let K be a compact space and $\boldsymbol{F}: K \to \mathbb{R}^k$ a continuous injection. Then $\boldsymbol{F}$ is a homeomorphism onto its image.

Note that the forward model $\boldsymbol{F_l}$ is only injective if regarded as a function over $\mathscr{P}_l$, and if the pickup coils provide enough information on the secondary magnetic field. For this purpose, they should not be placed redundantly and their number k has to be large enough compared to l. A rigorous mathematical proof of the forward model being injective is beyond the scope of this article.

D. Discussion and Further Remarks on Error Propagation

We found that the inverse problem of locating multiple passive 3-D coils is actually ill posed in general, but the ill posedness arises only from ambiguities of the projection onto the image of the forward model. If such ambiguities do not exist, the problem is well posed.

However, the third Hadamard condition is often interpreted more freely in the literature. Instead of just demanding continuity, the problem is also required to be well conditioned. In our context, this means that small observational errors do not affect the estimated 3-D coil positions too much. Methods from linear algebra are applied in the following in order to quantify this error propagation. For this purpose, we consider $\boldsymbol{F_l}(\boldsymbol{s_1^*}, \ldots, \boldsymbol{s_l^*})$ to be the error free measurement if l 3-D coils are located at $\boldsymbol{s_1^*}, \ldots, \boldsymbol{s_l^*}$. The forward model is regarded as a function on $P^l \subset \mathbb{R}^{3l}$ and approximated by its first-order Taylor polynomial at $\boldsymbol{x^*} = (\boldsymbol{s_1^*}, \ldots, \boldsymbol{s_l^*})$

$$\boldsymbol{F_l}(\boldsymbol{x}) \approx \boldsymbol{F_l}(\boldsymbol{x^*}) + D\boldsymbol{F_l}(\boldsymbol{x^*})(\boldsymbol{x} - \boldsymbol{x^*}) \tag{20}$$

where $D\boldsymbol{F_l}(\boldsymbol{x^*})$ denotes the Jacobian matrix of $\boldsymbol{F_l}$ evaluated at $\boldsymbol{x^*}$. Now let $\widetilde{\boldsymbol{b}} \approx \boldsymbol{F_l}(\boldsymbol{x^*})$ be a noisy measurement. Then the minimum point $\widetilde{\boldsymbol{x}}$ of

$$\|\boldsymbol{F_l}(\boldsymbol{x^*}) + D\boldsymbol{F_l}(\boldsymbol{x^*})(\boldsymbol{x} - \boldsymbol{x^*}) - \widetilde{\boldsymbol{b}}\|_2 \tag{21}$$

is a good approximation for the actual solution of the inverse problem for $\widetilde{\boldsymbol{b}}$. Minimizing (21) is actually a linear least squares problem and therefore easily achieved by means of the Moore–Penrose pseudoinverse $D\boldsymbol{F_l}(\boldsymbol{x^*})^+$ of $D\boldsymbol{F_l}(\boldsymbol{x^*})$ [27, Ch. 7.3]. This yields the following estimation for the propagated absolute localization error:

$$\begin{aligned}\|\widetilde{\boldsymbol{x}} - \boldsymbol{x^*}\|_2 &= \|D\boldsymbol{F_l}(\boldsymbol{x^*})^+(\widetilde{\boldsymbol{b}} - \boldsymbol{F_l}(\boldsymbol{x^*}))\|_2 \\ &\leq \|D\boldsymbol{F_l}(\boldsymbol{x^*})^+\|_2 \|\widetilde{\boldsymbol{b}} - \boldsymbol{F_l}(\boldsymbol{x^*})\|_2. \end{aligned} \tag{22}$$

So, the spectral norm $\|\cdot\|_2$ of $D\boldsymbol{F_l}(\boldsymbol{x^*})^+$ is an approximate upper bound for the amplification factor of measurement errors near $\boldsymbol{x^*}$. Regarding $\|D\boldsymbol{F_l}(\boldsymbol{x^*})^+\|_2$ as a function of $\boldsymbol{x^*}$ makes it possible to detect the regions where major localization errors have to be expected (see Section V).

IV. Localization Algorithm

In this section, a method for the localization of one or more passive 3-D coils is presented. In order to determine the 3-D coils' positions, we have to minimize the residual (18) which corresponds to solving a nonlinear least squares problem. For this purpose, we choose the Levenberg–Marquardt algorithm [31] due to its good results in practice [16], [32]. It calculates the minimum of (18) as the limit of a sequence $\{\boldsymbol{x_n}\}$ which is constructed iteratively by means of linearization. More precisely, $\boldsymbol{x_{n+1}}$ is obtained from $\boldsymbol{x_n}$ by minimizing

$$\|\boldsymbol{F_l}(\boldsymbol{x_n}) + D\boldsymbol{F_l}(\boldsymbol{x_n})(\boldsymbol{x} - \boldsymbol{x_n}) - \boldsymbol{b}\|_2^2 + \lambda\|\boldsymbol{x} - \boldsymbol{x_n}\|_2^2 \tag{23}$$

over $\boldsymbol{x} \in \mathbb{R}^{3l}$ with an adaptive damping parameter $\lambda > 0$. Finding the minimum of (23) is a linear least squares problem and therefore easily possible. The penalty term $\lambda\|\boldsymbol{x} - \boldsymbol{x_n}\|_2^2$ can be understood as a Tikhonov regularization enforcing $\boldsymbol{x_{n+1}}$ to be close to $\boldsymbol{x_n}$. Appropriate values for λ do not have to be chosen manually but are updated automatically after each iteration as follows: iteration steps with $\|\boldsymbol{F_l}(\boldsymbol{x_{n+1}}) - \boldsymbol{b}\|_2 > \|\boldsymbol{F_l}(\boldsymbol{x_n}) - \boldsymbol{b}\|_2$ are rejected and repeated with a bigger value for λ. On the other hand, λ is updated with a smaller value if the cost function (18) actually decreases as predicted by its linearization in $\boldsymbol{x_n}$. This adaptive choice of the damping parameter enables Levenberg–Marquardt to make smaller iteration steps when necessary.

The initial value $\boldsymbol{x_0}$ must be chosen manually. Note that even for $\boldsymbol{x_0} \in P^l$ the sequence $\{\boldsymbol{x_n}\}$ is not guaranteed to stay in P^l. However, this can be enforced by defining the values of $\boldsymbol{F_l}$ outside P^l as infinity. Since our forward model is rather complex, the Jacobian $D\boldsymbol{F_l}(\boldsymbol{x_n})$ in (23) is not computed analytically but approximated by a finite difference scheme. For deeper insights into the algorithm's performance numerical tests are performed in Section V.

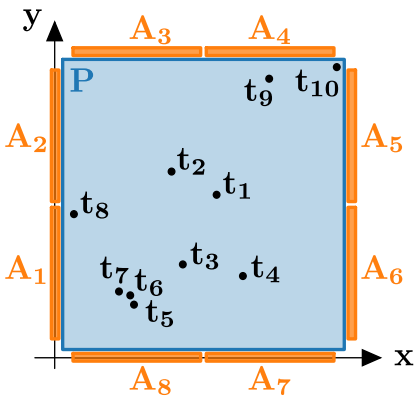

Fig. 4. 2-D localization setup with the pickup coils $A_1, \ldots, A_8$ and the test positions $\boldsymbol{t_1}, \ldots, \boldsymbol{t_{10}}$ in the localization area P.

V. Localization With Simulated Data

Our aim is to use Levenberg–Marquardt as a method for the 2-D localization of multiple passive 3-D coils within a wooden shelf. With this in mind, a simulation is carried out in the following in order to evaluate its performance and analyze the propagation of simulated Gaussian noise. The geometry of the setup can be described as follows: the exciter wire is a closed polygonal curve with the vertices (0 m, 0 m), (0.79 m, 0 m), (0.79 m, 0.79 m), (0 m, 0.79 m) around the localization area $P = [0.01\text{ m}, 0.78\text{ m}] \times [0.01\text{ m}, 0.78\text{ m}]$ and the surfaces of the pickup coils are:

$$\begin{aligned}
A_1 &= [-0.0085\text{ m}, 0.0085\text{ m}] \times [0.061\text{ m}, 0.39\text{ m}]\\
A_2 &= [-0.0085\text{ m}, 0.0085\text{ m}] \times [0.40\text{ m}, 0.729\text{ m}]\\
A_3 &= [0.061\text{ m}, 0.39\text{ m}] \times [0.7815\text{ m}, 0.7985\text{ m}]\\
A_4 &= [0.40\text{ m}, 0.729\text{ m}] \times [0.7815\text{ m}, 0.7985\text{ m}]\\
A_5 &= [0.7815\text{ m}, 0.7985\text{ m}] \times [0.40\text{ m}, 0.729\text{ m}]\\
A_6 &= [0.7815\text{ m}, 0.7985\text{ m}] \times [0.061\text{ m}, 0.39\text{ m}]\\
A_7 &= [0.40\text{ m}, 0.729\text{ m}] \times [-0.0085\text{ m}, 0.0085\text{ m}]\\
A_8 &= [0.061\text{ m}, 0.39\text{ m}] \times [-0.0085\text{ m}, 0.0085\text{ m}] \qquad (24)
\end{aligned}$$

(see Fig. 4) where the square brackets denote closed subintervals of $\mathbb{R}$, and $\times$ is the Cartesian product. Even though higher exciter frequencies f result in stronger signals at the pickup coils and therefore a higher signal-to-noise ratio, they also degrade the performance of our system due to increasing parasitic capacitive and inductive effects from surrounding obstacles. In addition, the shelf needs to meet the regulatory standards by the Federal Communications Commission (FCC). Therefore, we choose $f = 119$ kHz. The remaining model parameters are $I_{\text{ex}} = 1\,\text{A}$, $l_{\max} = 4$, $S = 1.7^2 \cdot \pi\ \text{cm}^2$, $R = 1\,\Omega$, and $M = N = 20$.

The ill posedness of our inverse source problem in this specific setting is evaluated by regarding the approximate upper bound for the localization error (22) for $l = 1$. The forward model is implemented in Python (Version 3.6) and $\|D\boldsymbol{F_1}(x, y)^+\|_2$ is plotted as a function of $(x, y) \in P$. Fig. 5 shows that sensitivity to observational noise increases with the distance to the pickup coils. Assuming a noise level of 0.01 mV one has to expect a localization error of about 3 cm near the center of P.

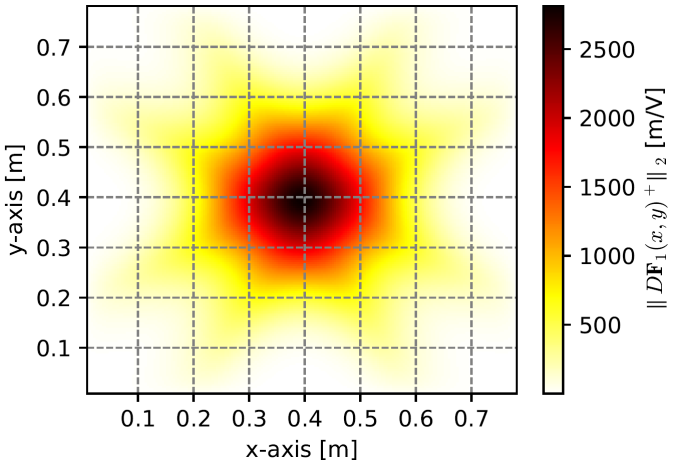

Fig. 5. Color plot of $\|D\boldsymbol{F_1}(x, y)^+\|_2$: as discussed in Section III-D our inverse problem is very ill conditioned in the dark area.

The Python library SciPy includes an implementation of Levenberg–Marquardt to be found at

```
scipy.optimize.least_squares(method='lm')
```

which is used for our computations with the termination criteria `ftol=1e-10` [change of the cost function (18)], `xtol=1e-10` (change of the variable $\boldsymbol{x}$), and `gtol=1e-10` (norm of the gradient). For further investigations, we select ten test positions covering a broad spectrum of possible scenarios

$$\begin{aligned}
\boldsymbol{t_1} &= (0.43\text{ m}, 0.42\text{ m}) \quad \boldsymbol{t_2} = (0.31\text{ m}, 0.48\text{ m})\\
\boldsymbol{t_3} &= (0.34\text{ m}, 0.24\text{ m}) \quad \boldsymbol{t_4} = (0.5\text{ m}, 0.21\text{ m})\\
\boldsymbol{t_5} &= (0.21\text{ m}, 0.136\text{ m}) \quad \boldsymbol{t_6} = (0.2\text{ m}, 0.16\text{ m})\\
\boldsymbol{t_7} &= (0.17\text{ m}, 0.17\text{ m}) \quad \boldsymbol{t_8} = (0.05\text{ m}, 0.37\text{ m})\\
\boldsymbol{t_9} &= (0.57\text{ m}, 0.72\text{ m}) \quad \boldsymbol{t_{10}} = (0.75\text{ m}, 0.75\text{ m}) \qquad (25)
\end{aligned}$$

(see Fig. 4) and generate model data as

$$\boldsymbol{b}_{i_1,\ldots,i_l} := \boldsymbol{F}_l(\boldsymbol{t}_{i_1}, \ldots, \boldsymbol{t}_{i_l}). \qquad (26)$$

Note that Levenberg–Marquardt should return the exact test positions when minimizing $\|\boldsymbol{F}_l(\boldsymbol{x}) - \boldsymbol{b}_{i_1,\ldots,i_l}\|_2$. This is indeed the case, e.g., for $\boldsymbol{b_{2,4,9}}$ and the initial value $\boldsymbol{x_0} = (0.395\text{ m}, \ldots, 0.395\text{ m}) \in \mathbb{R}^6$. However, taking a closer look at the required iteration steps in Fig. 6 shows that Levenberg–Marquardt prioritizes the 3-D coils closer to the pickup coils and thus tends to find them in a certain order instead of simultaneously. As a result, the forward model is evaluated unnecessarily often. We address this lack of efficiency by starting with the localization of only one 3-D coil and increasing their number step by step until the actual number of 3-D coils is reached. This also has the advantage that model evaluations are less expensive at the beginning. Consider Algorithm 1 for more details. If l is not known *a priori*, this algorithm can be modified easily so that it determines both the number and the positions of the 3-D coils. For this purpose, the 3-D coil number is increased as long as this results in an improvement, i.e., the minimum of (18) for $l + 1$ is smaller than its minimum for l (see Algorithm 2). By that, it is also possible to detect whether there are no 3-D coils in the localization area at all.

Algorithm 1 Localization With Known l

Input: measurement $\boldsymbol{b}$, 3D-coil number l

$\boldsymbol{x_0} = (0.395\,\text{m}, 0.395\,\text{m}) \in P$;
for $i = 1, ..., l$ **do**
  find the minimum $\boldsymbol{x}^*$ of $\|\boldsymbol{F_i}(\boldsymbol{x}) - \boldsymbol{b}\|_2$ for $\boldsymbol{x} \in P^i$ using Levenberg–Marquardt with initial value $\boldsymbol{x_0}$;
  set $\boldsymbol{x_0} = (\boldsymbol{x}^* \,|\, 0.395\,\text{m}, 0.395\,\text{m}) \in P^{i+1}$;
end
return $\boldsymbol{x}^* \in P^l$;

Output: 3D-coil positions $\boldsymbol{x}^*$

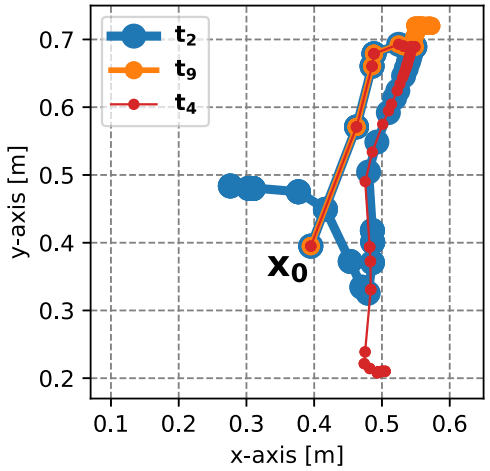

Fig. 6. Iteration steps of the Levenberg–Marquardt algorithm minimizing $\|\boldsymbol{F_3}(\boldsymbol{x}) - \boldsymbol{F_3}(\boldsymbol{t_2}, \boldsymbol{t_4}, \boldsymbol{t_9})\|_2$ over $\boldsymbol{x} \in P^3$.

TABLE I
CAPABILITY OF LEVENBERG–MARQUARDT TO RECONSTRUCT THE EXACT 3-D COIL POSITIONS FROM MODEL DATA

test positions	return of the exact test positions Alg. 1 / Alg. 2	required model evaluations Alg. 1 / Alg. 2
$\boldsymbol{t_1}$	yes / yes	13 / 47
$\boldsymbol{t_{10}}$	yes / yes	25 / 87
$\boldsymbol{t_3}$	yes / yes	26 / 91
$\boldsymbol{t_8}$	yes / yes	36 / 115
$\boldsymbol{t_5}$	yes / yes	37 / 107
$\boldsymbol{t_9}$	yes / yes	42 / 102
$(\boldsymbol{t_2}, \boldsymbol{t_4})$	yes / yes	73 / 188
$(\boldsymbol{t_1}, \boldsymbol{t_8})$	yes / yes	60 / 268
$(\boldsymbol{t_7}, \boldsymbol{t_9})$	yes / yes	85 / 187
$(\boldsymbol{t_5}, \boldsymbol{t_6})$	yes / yes	311 / 565
$(\boldsymbol{t_9}, \boldsymbol{t_{10}})$	yes / yes	817 / 1715
$(\boldsymbol{t_3}, \boldsymbol{t_4}, \boldsymbol{t_9})$	yes / yes	157 / 358
$(\boldsymbol{t_5}, \boldsymbol{t_8}, \boldsymbol{t_9})$	yes / yes	176 / 739
$(\boldsymbol{t_2}, \boldsymbol{t_4}, \boldsymbol{t_9})$	yes /yes	183 / 322
$(\boldsymbol{t_1}, \boldsymbol{t_2}, \boldsymbol{t_3})$	yes / yes	196 / 414
$(\boldsymbol{t_5}, \boldsymbol{t_6}, \boldsymbol{t_7})$	yes / yes	1359 / 1732
$(\boldsymbol{t_8}, \boldsymbol{t_9}, \boldsymbol{t_{10}})$	no / no	182 / 664
$(\boldsymbol{t_3}, \boldsymbol{t_4}, \boldsymbol{t_5}, \boldsymbol{t_8})$	yes / yes	250 / 250
$(\boldsymbol{t_2}, \boldsymbol{t_4}, \boldsymbol{t_6}, \boldsymbol{t_8})$	yes / yes	661 / 661
$(\boldsymbol{t_1}, \boldsymbol{t_2}, \boldsymbol{t_3}, \boldsymbol{t_4})$	no / no	295 / 295

Both algorithms are now tested with some of the model data defined in (26). Their performance is evaluated by counting how many evaluations of the forward model are required until termination. The results are shown in Table I. Both algorithms terminate in every test case and the global minimum of (18) is found for all model data generated by less than three 3-D coils. In the test cases $(\boldsymbol{t_8}, \boldsymbol{t_9}, \boldsymbol{t_{10}})$ and $(\boldsymbol{t_1}, \boldsymbol{t_2}, \boldsymbol{t_3}, \boldsymbol{t_4})$ both algorithms get trapped into a local minimum. Instead of the respective exact test positions they return

$$(0.050\ \text{m}, 0.370\ \text{m}), (0.421\ \text{m}, 0.604\ \text{m}), (0.756\ \text{m}, 0.761\ \text{m}) \tag{27}$$

and

$$(0.351\,\text{m}, 0.494\,\text{m}), (0.303\,\text{m}, 0.371\,\text{m}), (0.427\,\text{m}, 0.195\,\text{m}), (0.500\ \text{m}, 0.286\ \text{m}) \tag{28}$$

rounded to three decimal places. Whereas in the first of these two test cases the results for $\boldsymbol{t_8}$ and $\boldsymbol{t_{10}}$ are still quite accurate, there is no obvious relation between the test positions and the calculated ones in the second test case. Finally, the forward model is evaluated notably often in some cases when the 3-D coils are too close to the pickup coils or too close together. This indicates that Levenberg–Marquardt has to make very small iteration steps in order to converge.

Algorithm 2 Localization With Unknown l

Input: measurement $\boldsymbol{b}$

$\boldsymbol{x_0} = (0.395\,\text{m}, 0.395\,\text{m}) \in P$, $r = \|\boldsymbol{b}\|_2$, $\boldsymbol{x}^* = \texttt{None}$;
for $i = 1, ..., l_{max}$ **do**
  find the minimum $\widetilde{\boldsymbol{x}}$ of $\|\boldsymbol{F_i}(\boldsymbol{x}) - \boldsymbol{b}\|_2$ for $\boldsymbol{x} \in P^i$ using Levenberg–Marquardt with initial value $\boldsymbol{x_0}$;
  if $r < \|\boldsymbol{F_i}(\widetilde{\boldsymbol{x}}) - \boldsymbol{b}\|_2$ **then**
    return $\boldsymbol{x}^*$;
  end
  set $\boldsymbol{x}^* = \widetilde{\boldsymbol{x}}$, $r = \|\boldsymbol{F_i}(\boldsymbol{x}^*) - \boldsymbol{b}\|_2$, $\boldsymbol{x_0} = (\boldsymbol{x}^* \,|\, 0.395\,\text{m}, 0.395\,\text{m}) \in P^{i+1}$;
end
return $\boldsymbol{x}^*$;

Output: 3D-coil positions $\boldsymbol{x}^*$

TABLE II
PROPAGATION OF SIMULATED GAUSSIAN NOISE IN INDIVIDUAL AND SIMULTANEOUS LOCALIZATION

test positions	Euclidean norm of the mean absolute localization errors in each test position (in cm)	right-hand side of (22) (in cm)
$\boldsymbol{t_5}$	0.505	0.200
$\boldsymbol{t_4}$	0.876	0.691
$\boldsymbol{t_2}$	1.92	1.51
$(\boldsymbol{t_2}, \boldsymbol{t_4})$	$\sqrt{1.51^2 + 0.790^2} = 1.70$	1.69
$(\boldsymbol{t_4}, \boldsymbol{t_5})$	$\sqrt{1.49^2 + 0.844^2} = 1.71$	0.84
$(\boldsymbol{t_2}, \boldsymbol{t_5})$	$\sqrt{1.71^2 + 0.418^2} = 1.76$	1.68
$(\boldsymbol{t_2}, \boldsymbol{t_4}, \boldsymbol{t_5})$	$\sqrt{2.43^2 + 1.75^2 + 0.923^2} = 3.13$	1.90

We use a simple Monte Carlo method to investigate how the number of 3-D coils being located at the same time affects the propagation of observational errors: Gaussian noise $\boldsymbol{\varepsilon} \sim \mathcal{N}(\boldsymbol{0}, \sigma^2 \mathbb{1})$ is added to the model data $\boldsymbol{b}_{i_1,...,i_l}$ and the corresponding inverse problem is solved with Algorithm 1. From 400 such samples the mean absolute localization error is estimated in each test position belonging to $\boldsymbol{b}_{i_1,...,i_l}$. For this

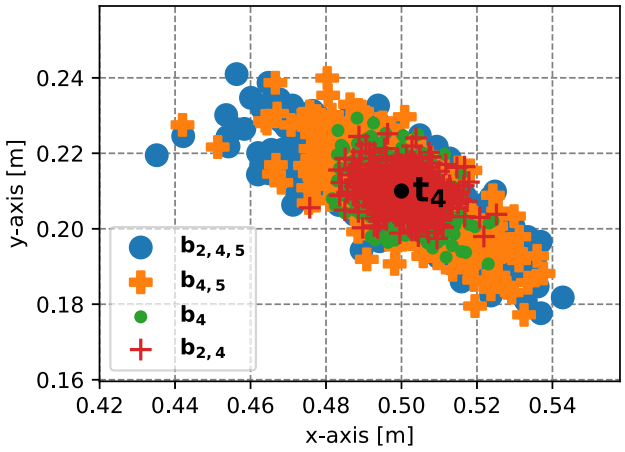

Fig. 7. Propagation of simulated measurement errors: 400 randomly generated Gaussian noise vectors with standard deviation $\sigma = 0.01$ mV are added to each of the model data $\boldsymbol{b_4}$, $\boldsymbol{b_{2,4}}$, $\boldsymbol{b_{4,5}}$, $\boldsymbol{b_{2,4,5}}$, and the corresponding inverse problems are solved with Algorithm 1. Only the estimated 3D-coil positions deviating from test position $\boldsymbol{t_4}$ are plotted.

sensitivity analysis, we select the test positions $\boldsymbol{t_2}$, $\boldsymbol{t_4}$, $\boldsymbol{t_5}$ and consider the model data $\boldsymbol{b_2}$, $\boldsymbol{b_4}$, $\boldsymbol{b_5}$, $\boldsymbol{b_{2,4}}$, $\boldsymbol{b_{2,5}}$, $\boldsymbol{b_{4,5}}$, $\boldsymbol{b_{2,4,5}}$. With respect to the noise level at the real setup we set $\sigma = 0.01$ mV. In order to verify the validity of the approximate upper bound for the localization error from Section III, the right-hand side of (22) is evaluated for $\|\widetilde{\boldsymbol{b}} - \boldsymbol{F_l}(\boldsymbol{x^*})\|_2 = 0.01$ mV and compared to the Euclidean norm of the mean absolute localization errors in each test position. The results are shown in Table II and Fig. 7. As expected, the localization errors increase with the test positions' distance to the pickup coils. It is remarkable that the simultaneous localization of two 3-D coils from $\boldsymbol{b_{i_1,i_2}} + \boldsymbol{\varepsilon}$ is not necessarily more—or even less—sensitive to noise than their individual localization from $\boldsymbol{b_{i_1}} + \boldsymbol{\varepsilon}$ and $\boldsymbol{b_{i_2}} + \boldsymbol{\varepsilon}$. However, for all test positions the maximum mean localization error occurs when the three passive 3-D coils are located simultaneously from $\boldsymbol{b_{2,4,5}} + \boldsymbol{\varepsilon}$. The right-hand side of (22) turns out to be a powerful tool for predicting the localization error's order of magnitude. However, in some test cases the sampled localization error is less consistent with the predicted one than in others which indicates that the model is not very well approximated by its linearization in the respective test positions.

VI. Localization With Experimental Data

Both localization methods from Section V are now applied to a wooden shelf equipped with the IndLoc positioning technology by the Fraunhofer Institute for Integrated Circuits. The exciter wire and eight pickup coils are placed around the square front of this shelf as shown in Fig. 8. A reader connected to a PC via ethernet both supplies the exciter wire with electric current and processes the received signals. For a more detailed description of the setup see [6]. Fig. 9 shows a 3-D coil being placed in one of the 16 equally sized compartments of the shelf. All 3-D coils have 1.7-cm radius and are tuned to the resonance frequency 119 kHz by capacitors. To make sure that we only measure the secondary magnetic field generated by the 3-D coils, the offset is determined after removing all objects from the localization area and subtracted from the signals. Despite their identical design the pickup

Fig. 8. Wooden shelf with 16 compartments surrounded by an exciter wire and eight pickup coils around its square front. The exciter wire goes through the white plastic elements and the pickup coils are winded around them.

Fig. 9. 3-D coil consisting of three orthogonal identically winded circular coils which are tuned to resonance by capacitors (covered by a turquoise heat shrink tubing).

coils have to be calibrated in phase and magnitude to receive comparable signals. For this purpose, we divide each signal by a reference signal which is generated by a ferrite object being held directly at the respective pickup coil. As a negative side effect of this calibration the signals are rescaled and therefore not directly comparable to our model data. Consequently, also the forward model from Section V needs to be rescaled with a constant factor γ which is determined empirically as the arithmetic mean of the following quotients:

$$\frac{\boldsymbol{b}^i_j}{\boldsymbol{F_1}(\boldsymbol{c_i})_j}, \quad i = 1, \ldots, 16, \quad j = 1, \ldots 8 \tag{29}$$

where $\boldsymbol{c_i}$ denotes the center of the ith shelf compartment, $\boldsymbol{F_1}(\boldsymbol{c_i})_j$ the jth entry of the model data $\boldsymbol{F_1}(\boldsymbol{c_i})$ and $\boldsymbol{b}^i_j$ the real measurement at the jth pickup coil if a single 3-D coil is placed in the center of the ith shelf compartment as shown in Fig. 9. This yields the following value for our setup being multiplied to $\boldsymbol{F_l}$:

$$\gamma \approx 17.82 \tag{30}$$

(see Fig. 10). Note that the values of $\|D\boldsymbol{F_1}(x, y)^+\|_2$ in Fig. 4 have to be divided by γ in order to be consistent with the rescaled model.

Based on (22) and [7], the total dipole moment of a 3-D coil is assumed to be invariant under rotation. In order to empirically verify whether this approximation is justified, a 3-D

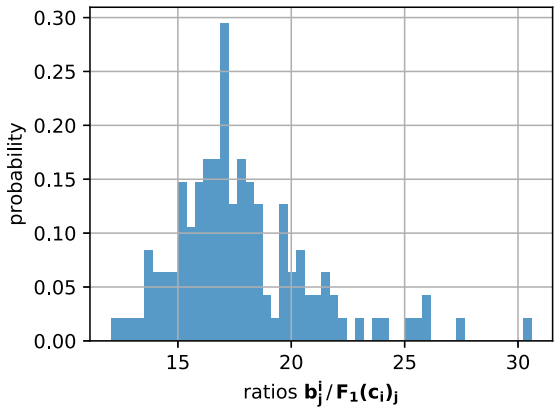

Fig. 10. Histogram of all 128 ratios defined in (29) with mean value 17.82 and standard deviation 3.075.

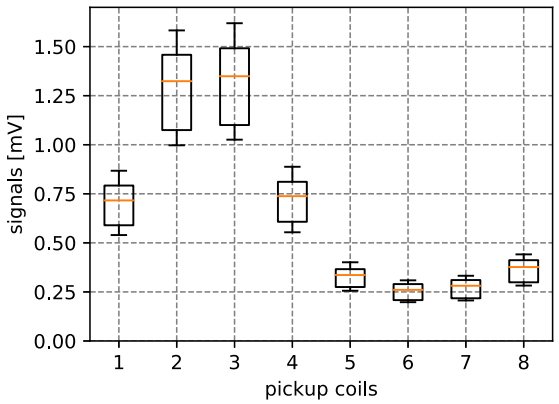

Fig. 11. Empirical examination of the secondary magnetic field's invariance under rotation of the 3-D coils: a 3-D coil is placed at the center of the sixth shelf compartment with ten different orientations and the corresponding signals at the pickup coils are visualized as a box plot.

coil is placed in the middle of the sixth shelf compartment and randomly rotated ten times. Fig. 11 shows the discrepancies of the resulting measurements. The same procedure is repeated in the compartments one, two, and five obtaining a series of 32×10 measurements in total. From these values, it is calculated that the standard deviation of the signals measured by one pickup coil roughly corresponds to 13 % of the respective mean signal value. The discrepancy between this rather large percentage and the invariance of the signals under rotation of the 3-D coils as predicted by our model arises from the primary magnetic field's linear approximation (3) as well as the approximation of each 3-D coil as a magnetic dipole (see also [7] for a more comprehensive analysis). Despite this model error, our method still provides reasonable estimates for the 3-D coil positions. More precisely, the ten different 3-D coil orientations in the compartments one, two, five, and six result in mean absolute localization errors of 1.2, 1.6, 2.0, and 3.6 cm, respectively. Better results are obtained if the signals are treated relatively as percentages of the total signal measured by all eight pickup coils together even if information gets lost by that. For this purpose, the cost function (18) is replaced by

$$\left\| \frac{\boldsymbol{F_l}(\boldsymbol{x})}{\|\boldsymbol{F_l}(\boldsymbol{x})\|_1} - \frac{\boldsymbol{b}}{\|\boldsymbol{b}\|_1} \right\|_2 \tag{31}$$

where $\|\boldsymbol{b}\|_1 = \sum_{i=1}^{8} |\boldsymbol{b_i}|$ denotes the ℓ_1-norm. With this relative residual the ten different 3-D coil orientations in the compartments one, two, five, and six result in mean absolute localization errors of 0.9, 0.8, 1.2, and 0.2 cm, respectively.

TABLE III
LOCALIZATION ERRORS AND NUMERICAL EFFORT WITH REAL DATA

	number of 3D-coils l	1	2	3
Algorithm 1 with (18)	mean absolute localization error	1.3 cm	1.8 cm	4.7 cm
	mean number of model evaluations	29	106	263
Algorithm 1 with (31)	mean absolute localization error	0.9 cm	1.2 cm	3.8 cm
	mean number of model evaluations	20	105	198
Algorithm 2	mean absolute localization error	1.3 cm	1.8 cm	4.7 cm
	mean number of model evaluations	96	228	263

Now a maximum of three passive 3-D coils is placed centrally in different compartments of the shelf as shown in Fig. 9 and both algorithms from Section V are applied in order to estimate their number and positions. With this *a priori* knowledge, we set $l_{\max} = 3$. The mean absolute localization error is determined over all test scenarios with a fixed number l of 3-D coils being in the shelf at the same time. For $l = 1$, this is done in all 16 compartments. For the cases $l = 2$ and $l = 3$, we restrict ourselves to 32 and 39 combinations of two and three compartments being equipped with a 3-D coil at the same time. More is also not necessary due to the fourfold symmetry of the shelf. Whereas Algorithm 1 works with both cost functions (18) and (31), Algorithm 2 requires absolute signal values since

$$\frac{\boldsymbol{F_1}(\boldsymbol{s})}{\|\boldsymbol{F_1}(\boldsymbol{s})\|_1} = \frac{\boldsymbol{F_2}(\boldsymbol{s},\boldsymbol{s})}{\|\boldsymbol{F_2}(\boldsymbol{s},\boldsymbol{s})\|_1} = \frac{\boldsymbol{F_3}(\boldsymbol{s},\boldsymbol{s},\boldsymbol{s})}{\|\boldsymbol{F_3}(\boldsymbol{s},\boldsymbol{s},\boldsymbol{s})\|_1} \tag{32}$$

holds for all $\boldsymbol{s} \in P$ which is a consequence of (14). The results are presented in Table III. Apparently, Algorithm 1 is more precise when using relative signal values. Since Algorithm 2 also estimates the number of 3-D coils in the localization area, it requires more evaluations of the forward model. However, the estimated number of 3-D coils is always correct. Even though the mean absolute localization error for $l = 3$ is almost three times larger than the radius of the 3-D coils, their positions are always estimated within the right compartment of the shelf. Note that the discrepancy between real and model data does not only arise from measurement noise but also from the fact that our forward model is a simplification of reality. In this context, we recall that the 3-D coils are treated as magnetic dipoles and the calculation of their dipole moments is based on the approximation of the primary field by its linearization in their centers. Also the inductive coupling between the individual 3-D coils is neglected as well as the magnetic fields generated by the pickup coils. This explains why the localization errors in Table II tend to be smaller than in Table III.

VII. CONCLUSION

In this article, it was shown that multiple passive 3-D coils whose electric currents are induced externally by a low-frequency magnetic field can be located without separating

their signals. The Biot–Savart law was used to describe the primary magnetic field and the 3-D coils were approximated as magnetic dipoles whose dipole moments are invariant under rotation. This enabled the formulation of their localization as an inverse problem which turned out to be ill posed for two reasons: first, the underlying optimization problem has more than one solution if the pickup coils do not provide enough information, and second, the localization suffers from strong sensitivity to observational noise. With regard to the latter an approximate upper bound for the propagated localization error was derived by linearizing the inverse problem and applying the Moore–Penrose pseudoinverse. By that, especially regions further away from the pickup coils were detected to be problematic. The Levenberg–Marquardt algorithm was introduced as a method for localization. Gradually increasing the number of 3-D coils in its initial value improved the algorithm's performance and made it possible to estimate the actual number of 3-D coils in the localization area. Tests were performed in order to verify the algorithm's functionality as a method for 2-D localization within the front of a wooden shelf by means of eight pickup coils. In a numerical simulation Levenberg–Marquardt was able to reconstruct the exact 3-D coil positions from model data but the localization of four 3-D coils at the same time turned out to be impractical. A Monte Carlo sensitivity analysis showed that locating two 3-D coils simultaneously instead of individually can affect the propagation of simulated Gaussian noise both in a positive and in a negative way. At the real test setup the orientations of the 3-D coils turned out to have more impact on the measurements than expected. Even if localization is still possible, its accuracy can be improved by transforming the absolute signals into relative values. However, this is only possible if the number of 3-D coils in the localization area is known. In both cases, we were able to locate up to three passive 3-D coils at the same time with an accuracy of just a few centimeters which is roughly the size of a 3-D coil or 1:50 of the shelf's edge length.

REFERENCES

[1] D. Battini, M. Calzavara, A. Persona, and F. Sgarbossa, "A comparative analysis of different paperless picking systems," *Ind. Mangement Data Syst.*, vol. 115, no. 3, pp. 483–503, Apr. 2015.

[2] B. Schwerdtfeger *et al.*, "Pick-by-vision: A first stress test," in *Proc. 8th IEEE Int. Symp. Mixed Augmented Reality*, Orlando, FL, USA, vol. 92, 2009, pp. 115–124.

[3] S. Tumanski, "Induction coil sensors—A review," *Meas. Sci. Technol.*, vol. 18, no. 3, pp. R31–R46, Mar. 2007.

[4] R. Psiuk, T. Seidl, W. Strauß, and J. Bernhard, "Analysis of goal line technology from the perspective of an electromagnetic field based approach," *Procedia Eng.*, vol. 72, pp. 279–284, Jan. 2014.

[5] R. Psiuk, A. Artizada, D. Cichon, H. Brauer, H. Toepfer, and A. Heuberger, "Modeling of an inductively coupled system," in *COMPEL Int. J. Comput. Math. Electr. Electron. Eng.*, vol. 37, no. 4, pp. 1500–1514, Aug. 2018.

[6] R. Psiuk *et al.*, "Simultaneous 2D localization of multiple coils in an LF magnetic field using orthogonal codes," in *Proc. IEEE SENSORS*, Glasgow, U.K., Oct./Nov. 2017, pp. 1–3.

[7] R. Psiuk, A. Müller, D. Cichon, A. Heuberger, H. Brauer, and H. Töpfer, "Inductive localization accuracy of a passive 3-D coil in an industry 4.0 environment," *J. Sensors Sensor Syst.*, vol. 8, no. 1, pp. 171–183, Apr. 2019.

[8] V. Schlageter, P.-A. Besse, R. Popovic, and P. Kucera, "Tracking system with five degrees of freedom using a 2D-array of Hall sensors and a permanent magnet," *Sens. Actuators A, Phys.*, vol. 92, nos. 1–3, pp. 37–42, Aug. 2001.

[9] S. Baillet, J. Mosher, and R. Leahy, "Electromagnetic brain mapping," *IEEE Signal Process. Mag.*, vol. 18, no. 6, pp. 14–30, Nov. 2001.

[10] T. Nara, S. Suzuki, and S. Ando, "A closed-form formula for magnetic dipole localization by measurement of its magnetic field and spatial gradients," *IEEE Trans. Magn.*, vol. 42, no. 10, pp. 3291–3293, Oct. 2006.

[11] G. Dumphart, E. Slottke, and A. Wittneben, "Robust near-field 3D localization of an unaligned single-coil agent using unobtrusive anchors," in *Proc. IEEE 28th Annu. Int. Symp. Pers., Indoor, Mobile Radio Commun.(PIMRC)*, Montreal, QC, Canada, 2017, pp. 1–7.

[12] W. Kim, J. Song, and F. C. Park, "Closed-form position and orientation estimation for a three-axis electromagnetic tracking system," *IEEE Trans. Ind. Electron.*, vol. 65, no. 5, pp. 4331–4337, May 2018.

[13] C. Hu, S. Song, X. Wang, M. Q.-H. Meng, and B. Li, "A novel positioning and orientation system based on three-axis magnetic coils," *IEEE Trans. Magn.*, vol. 48, no. 7, pp. 2211–2219, Jul. 2012.

[14] B. R. Daniels, R. Pratt, R. Giaquinto, and C. Dumoulin, "Optimizing accuracy and precision of micro-coil localization in active-MR tracking," *Magn. Reson. Imag.*, vol. 34, no. 3, pp. 289–297, Apr. 2016.

[15] S. Hashi, S. Yabukami, H. Kanetaka, K. Ishiyama, and K. I. Arai, "Wireless magnetic position-sensing system using optimized pickup coils for higher accuracy," *IEEE Trans. Magn.*, vol. 47, no. 10, pp. 3542–3545, Oct. 2011.

[16] C. Hu, M. Q. Meng, and M. Mandal, "Efficient magnetic localization and orientation technique for capsule endoscopy," in *Proc. IEEE/RSJ Int. Conf. Intell. Robots Syst.*, Edmonton, AB, Canada, 2005, pp. 628–633.

[17] D. Cichon, R. Psiuk, H. Brauer, and H. Topfer, "A Hall-sensor-based localization method with six degrees of freedom using unscented Kalman filter," *IEEE Sensors J.*, vol. 19, no. 7, pp. 2509–2516, Apr. 2019.

[18] A. Sheinker, B. Ginzburg, N. Salomonski, L. Frumkis, and B.-Z. Kaplan, "Localization in 3-D using beacons of low frequency magnetic field," *IEEE Trans. Instrum. Meas.*, vol. 62, no. 12, pp. 3194–3201, Dec. 2013.

[19] H. Haneishi, N. Ohyama, K. Sekihara, and T. Honda, "Multiple current dipole estimation using simulated annealing," *IEEE Trans. Biomed. Eng.*, vol. 41, no. 11, pp. 1004–1009, Nov. 1994.

[20] J.-R. Regue, M. Ribo, J.-M. Garrell, and A. Martin, "A genetic algorithm based method for source identification and far-field radiated emissions prediction from near-field measurements for PCB characterization," *IEEE Trans. Electromagn. Compat.*, vol. 43, no. 4, pp. 520–530, Nov. 2001.

[21] Y. Vives-Gilabert, C. Arcambal, A. Louis, F. De Daran, P. Eudeline, and B. Mazari, "Modeling magnetic radiations of electronic circuits using near-field scanning method," *IEEE Trans. Electromagn. Compat.*, vol. 49, no. 2, pp. 391–400, May 2007.

[22] Y. Vives-Gilabert, C. Arcambal, A. Louis, P. Eudeline, and B. Mazari, "Modeling magnetic emissions combining image processing and an optimization algorithm," *IEEE Trans. Electromagn. Compat.*, vol. 51, no. 4, pp. 909–918, Nov. 2009.

[23] L. Beghou, B. Liu, L. Pichon, and F. Costa, "Synthesis of equivalent 3-D models from near field measurements—Application to the EMC of power printed circuit boards," *IEEE Trans. Magn.*, vol. 45, no. 3, pp. 1650–1653, Mar. 2009.

[24] Z. Yu, C. Xiao, H. Wang, and Y. Zhou, "The calculation of the magnetic field produced by an arbitrary shaped current-carrying wire in its plane," *Adv. Mater. Res.*, vols. 756–759, pp. 3687–3691, Sep. 2013.

[25] C. K. Alexander and M. N. O. Sadiku, *Fundamentals of Electric Circuits*, 4th ed. New York, NY, USA: McGraw-Hill, 2007, ch. 14.5, pp. 629–634.

[26] D. Halliday, R. Resnick, and J. Walker, *Fundamentals of Physics Extended*, 10th ed. Hoboken, NJ, USA: Wiley, 2013, ch. 29.5, pp. 851–854.

[27] G. Strang, *Introduction to Linear Algebra*, 5th ed. Cambridge, MA, USA: Wellesley-Cambridge, 2016, ch. 4.4 and 7.3, pp. 230–243 and 399–408.

[28] S. Willard, *General Topology*. Reading, MA, USA: Addison-Wesley, 1970, ch. 9 and 17, pp. 59–69 and 116–129.

[29] J. Hadamard, *Sur les Problèmes aux Dérivées Partielles et Leur Signification Physique*, vol. 13. Princeton, NJ, USA: Princeton Univ. Press, 1902, pp. 49–52.

[30] W. Rudin, *Principles of Mathematical Analysis*, 3rd ed. New York, NY, USA: McGraw-Hill, 1976, pp. 89–90.

[31] J. J. More, "The Levenberg–Marquardt algorithm: Implementation and theory," in *Numerical Analysis* (Lecture Notes in Mathematics), vol. 630, G. A. Watson, Ed. Berlin, Germany: Springer, 1978.

[32] R. G. De P. Menendez and S. L. G. Andino, "Single dipole localization: Some numerical aspects and a practical rejection criterion for the fitted parameters," *Brain Topography*, vol. 6, no. 4, pp. 277–282, Jun. 1994.